Effects of the organic additives on phase transformation and luminescence of Eu^{3+}-doped YPO_4 nano/microparticles

JINRONG BAO[*,a], XIAOWEI ZHU[b], GUOLEI ZHI[a], CHANGFU LI[a], SONGLIANG HE[a], WENXIAN LI[a], RANBO YU[*,c]
[a]*School of Chemistry and Chemical Engineering, University of Inner Mongolia, Hohhot 010021, China*
[b]*College of Pharmacology, Inner Mongolia Medical University, Hohhot 010059, China*
[c]*Department of Physical Chemistry, University of Science and Technology Beijing, Beijing 100 083, China*

YPO_4 nano/microparticles doped with Eu^{3+} (5 at. %) have been synthesized by hydrothermal route inducing organic additives citrite/oxalate, which acts as capping agent. It has been found that the varying the concentration of organic additives ions induces YPO_4:Eu^{3+} a phase transformation from tetragonal to hexagonal, and also a significant decrease in Eu^{3+} luminescence intensity was observed. This is related to the association of the water molecules in the hexagonal phase of YPO_4. The luminescent properties of YPO_4:Eu^{3+} prepared with different organic additives-induced have been compared. The ratio of the intensity of electronic dipole transition $^5D_0$-$^7F_2$ to the magnetic dipole transition $^5D_0$-$^7F_1$ for hexagonal YPO_4:Eu^{3+} prepared with oxalate-introduce is higher than that prepared with citrate-introduce.

(Received September 20, 2016; accepted November 28, 2017)

Keywords: Hexagonal YPO_4:Eu^{3+}, Luminescence, Phase tranformation, Microstructure

1. Introduction

Rare earth orthophosphates ($REPO_4$) have been widely used as high performance luminescent devices, magnets, catalysts, time-resolved fluorescence labels for biological detection [1-4]. In recent years, much interest has been focused on the synthesis and luminescence of nano-sized rare earth orthophosphates for the important advantages than on their potential application when compared with other available luminescent materials (quantum dots or organic dyes), such as low toxicity, photostability, high working temperature, and narrow emission lines and long emission lifetime [5,6].

Rare earth orthophosphates were found to exist in monoclinic, tetragonal and hexagonal phases [7-9]. $REPO_4$ (RE=La-Dy) have a hexagonal structure and (Ho-Lu, Y)PO_4 crystallize in a tetragonal structure under the same synthetic conditions. At low temperature, it has a hexagonal phase and can be transformed into monoclinic structure at high temperature [10,11]. Tetragonal YPO_4 could be easily obtained, it have been synthesized by various chemical synthesis including hydrothermal method [12], microwave-assisted method [13], liquid-solid-solution solvothermal method [14], high-boiling organic solvothermal method [15], and solid state reaction [16]. Hexagonal YPO_4 nanorods were synthesized through increasing Ce^{3+} doping ions concentrations [17] and Bi^{3+} doping ions concentrations [18]. Very recently, a variety of organic additives as the stabilizer and structure-inducing agent to control the crystal size, shape and structure was reported. Various complexing agents such as oleic acid [19], EDTA [20], citric acid [21] have been used in the synthesis. For example, Di *et al.* [22] used a citrate-mediated method to synthesize $TbPO_4$:Eu nanoparticles. Despite these efforts, important issues, the exploration of the key factors governing the evolution of crystal structure, are still in need of in-depth investigation. Before we started to work on this subject, a lot of effort had been devoted to the facile approach to control the shape and the crystal structure of $REPO_4$. By only increasing the concentration of oxalate/phosphate, the phase transformation of as-synthesized $CePO_4$ from the hexagonal to the monoclinic could be achieved at hydrothermal 100 - 150 °C [23,24].

In this work, the phase transformation of YPO_4:Eu from the tetragonal to the hexagonal could be achieved by the oxalate/citrate/benzoate-induced route. The evolution mechanism of the crystal structure was also proposed based on the comparative experiment. Then we concentrate on the luminescence properties of YPO_4:Eu particles with different structures and sizes.

2. Experimental sections

Morphology, structure and composition of the products were characterized by field-emission scanning electron microscopy (FE-SEM, S-4800), and X-ray diffractometry (XRD, M21XVHF22, MAC science Co.,

Ltd.), and thermogravimetry–differential thermal analyses (TG–DSC, Perkin Elmer TGA 4000), and Fourier transform infrared spectroscopy (Nicolet NEXUS 670 FT–IR). The photoluminescence spectra of powders were recorded on FL Spectrophotometer (FLS-920) at room temperature.

All chemicals were of analytical grade and were used as received without further purification. In a typical synthesis process, 9.5 mmol of $Y(NO_3)_3 \cdot 6H_2O$ and 0.5 mmol of $Eu(NO_3)_3 \cdot 6H_2O$ were dissolved in 10 mL of water (atomic ratio: Y/Eu = 9.5/0.5). The above mixture solution was added into 20 mL aqueous solution containing a certain amount of organic additive (sodium citrate $Na_3C_6H_5O_7 \cdot 2H_2O$ labeled as Cit^{3-}, ammonium oxalate $(NH_4)_2C_2O_4$ labeled as $C_2O_4^{2-}$). After stirring for about 30 min, 1.0 mol/L orthophosphoric acid solution was added. Then the solution was transferred into a 50mL autoclave, which was filled with deionized water up to 80 % capacity, sealed, and heated at 150 °C for 12 h. After cooling down the autoclave to room temperature, the precipitation was separated by centrifugation, washed with deionized water and ethanol several times, and then dried at 60 °C.

3. Results and discussion

3.1. XRD study

The crystal structure and the phase purity of the products have been identified by the X-ray diffraction analysis (XRD). Fig. 1 showed the XRD patterns of the as-synthesized $YPO_4:Eu^{3+}$ prepared with without organic additives and different amount of organic additives. The typical XRD pattern of the product prepared without organic additives was shown in Fig. 1a. All reflection peaks of it agree well with tetragonal YPO_4 ([space group *I*41 (141), PDF card No. 83–658]). Fig. 1b,c were the XRD patterns of the products prepared with different concentration of Cit^{3-}. When the concentration of Cit^{3-} was 0.2 mmol, the mixed tetragonal and hexagonal phase appeared (Fig. 1b). While the concentration of Cit^{3-} increased to 0.5 mmol, the hexagonal phase $YPO_4 \cdot 0.8H_2O$ appeared. All diffraction peaks agree well with a hexagonal phase $YPO_4 \cdot 0.8H_2O$ [space group $P3_121$ (152), PDF card No. 42-82] (Fig. 1c). A further increase the concentration of Cit^{3-} leads to the formation of hexagonal phase $YPO_4 \cdot 0.8H_2O$ (Fig. S1). Fig. 1d-g showed the XRD patterns of the products prepared with different concentration of $C_2O_4^{2-}$. When the concentration of $C_2O_4^{2-}$ was from 0.2 to 0.5 mmol, the mixed tetragonal and hexagonal phase appeared (Fig. 1d,e). Subsequently the concentration of $C_2O_4^{2-}$ increased to 0.7 mmol, the yttrium oxalate hydrate and hexagonal phase $YPO_4 \cdot 0.8H_2O$ could be detected (Fig. 1f). By the hydrothermal treatment for 24h, the pure hexagonal phase $YPO_4 \cdot 0.8H_2O$ was prepared, no yttrium oxalate hydrate could be observed (Fig. 1g). All reflection peaks could be indexed to hexagonal $YPO_4 \cdot 0.8H_2O$, no other impurities could be observed. The results indicate that ammonium oxalate coordinate with Y^{3+} ions to form intermediate ($Y_2(C_2O_4)_3$). Moreover, the coordination ability of oxalate as an organic ligand with Y^{3+} ions is stronger than that of citrate.

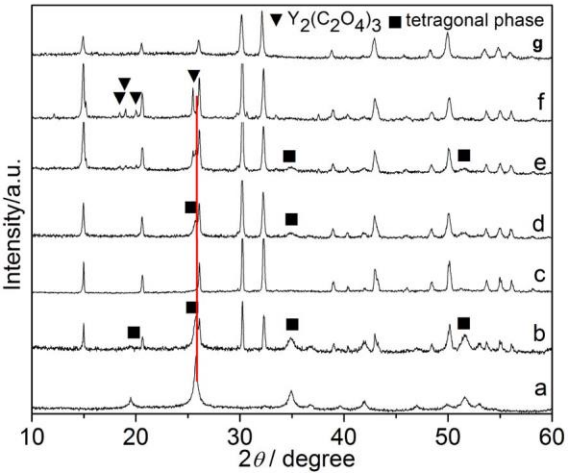

Fig. 1. XRD patterns of YPO_4Eu^{3+} products prepared with different concentration of organic additives for 12h: (a) without organic additives, (b,c) 0.2 and 0.5 mmol Cit^{3-}, (d-f) 0.2, 0.5 and 0.7 mmol $C_2O_4^{2-}$, (g) 0.7 mmol $C_2O_4^{2-}$, reaction time in crested to 24h

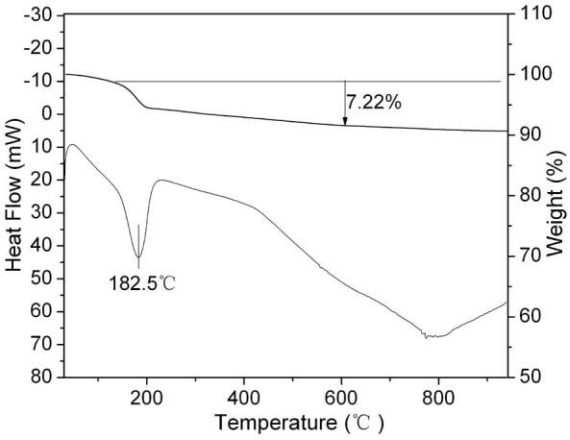

Fig. 2. TG-DSC plot of the hexagonal $YPO_4:Eu^{3+}$ prepared with 0.5 mmol citrate

The thermogravimetric analysis further confirmed the hydrated nature of the derived hexagonal yttrium phosphate prepared with citrate-introduced (Fig. 2). The weight loss occurs in two steps. The first one, below 136 °C, was associated with the release of residual water adsorbed on the powder surface due to the storage conditions in air. The second, in the 140 - 220 °C range, corresponded to the progressive dehydration of the hexagonal phase and was accompanied by an endothermic peak. The weight loss of 7.20 % resulting from the dehydration means about 0.8 mol H_2O in the $YPO_4 \cdot nH_2O$.

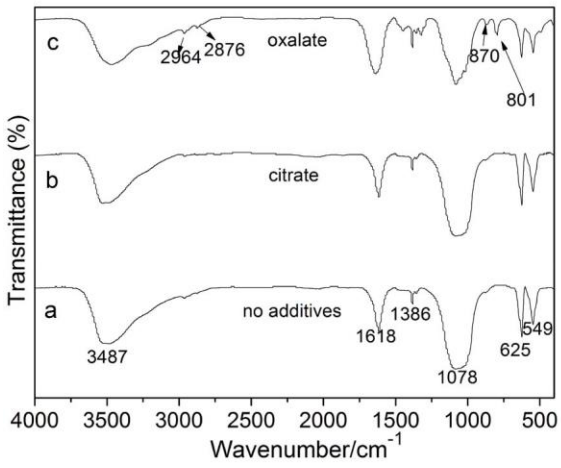

Fig. 3. FTIR spectra of YPO_4 prepared with different organic additives: (a) without organic additives, (a) 0.5 mmol Cit^{3-} and (b) 0.7 mmol $C_2O_4^{2-}$ (24h)

3.2. FTIR study

Moreover, FT-IR spectra of as-prepared tetragonal phase and hexagonal phase $YPO_4:Eu^{3+}$ were performed (Fig. 3). Three distinct IR peaks are observed at about 1078, 625, and 549 cm^{-1}, which are assigned to P–O stretching, P–O bending, and O–P–O bending mode of vibration, respectively [25]. The band around 1400 cm^{-1} corresponds to the vibration of residual NO_3^- groups [26] originating from the starting reactants ($Y(NO_3)_3$). The absorption band of around 3487 cm^{-1} is due to –OH stretch and the peak around 1618 cm^{-1} is attributed to –OH bending mode [27,28]. The absorption bands centered at 2964 and 2876 cm^{-1} (υCH_3 and υCH_2) can be attributed to the characteristic frequencies of residual ammonium oxalate, which indicate that there is still little amount of yttrium oxalate remaining in a sample prepared with ammonium oxalate [29].

3.3. FE-SEM study

The morphology of the as-synthesized products were investigated using FE-SEM (Fig. 4). As showed in Fig. 4a, the obtained sample synthesized without Cit^{3-} and $C_2O_4^{2-}$, an inhomogeneous nanoparticles were obtained, which are about 20 - 50 nm in diameter. Furthermore, when the concentration of Cit^{3-} was increasing to 2.2 mmol, the product is uniform hexagonal prisms with the each side about 200 nm and highness of about 200 - 300 nm, which were have uniform shapes (Fig. 4b,c). When the concentration of $C_2O_4^{2-}$ was 0.7 mmol, the inhomogeneous rod-like particles with a width of about 200 - 300 nm and a length of about 1-2 μm was formed (Fig 4d). The use of oxalate as organic additives gave rise to irregular particles, and larger sizes. We consider that the oxalate would coordinate with Y^{3+} ions to form intermediate ($Y_2(C_2O_4)_3$), and thus the concentration of Y^{3+} ions in the reaction system is relatively low. It decreases the nucleation rate and nucleation number of YPO_4, causing the size of the product to grow. Whereas Cit^{3-}/Y^{3+} molar ratio was from 2.2 to 3.0, uniform hexagonal prisms was obtained. The amount of the Cit^{3-} was found to be a key factor for the preparation of uniform hexagonal prisms.

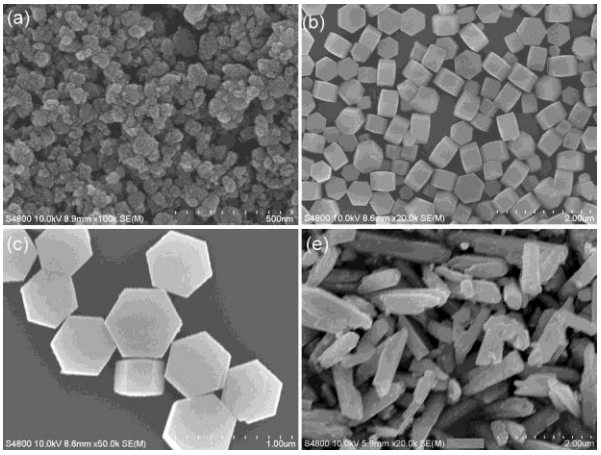

Fig. 4. FE-SEM images of $YPO_4:Eu^{3+}$ products prepared with different concentration of organic additives: (a) without organic additives, (b,c) 2.2 mmol Cit^{3-}, (d) 0.7 mmol $C_2O_4^{2-}$ (24h)

Comparative experiments were carried out to investigate the influences of the amount of the Cit^{3-} on the size and morphology of the products. The growth process was studied by the amount dependent observation using the XRD patterns and FE-SEM images (Fig. 5 and Fig. 6). Without the addition of citrate while keeping other conditions, mainly small particles with diameters of 20 - 50 nm were observed (Fig. 5a). When the reaction proceeds at the citrate concentration of 0.5 mmol, the product was composed of microparticles with diameters of about 1 μm (Fig. 5b). While was higher than 1.0, an interesting hexagonal-like microparticles with a 2 - 5 μm in diameter was formed (Fig. 5c). The concentration of citrate increasing from 2.0 to 2.2 mmoL, the uniform hexagonal prisms with a 200 - 400 nm in diameter was observed (Fig. 5d,e). Upon increasing the citrate amount to 5.0 mmoL, the corresponding morphology dramatically appears as sphere-like nanostructures with diameter about 100 nm (Fig. 5f). Generally, $LnPO_4$ tend to grow as 1D nanowires, which is possibly due to the 1D characteristics of the infinite linear chains of hexagonal structured $LnPO_4$ (Ln = La–Dy). On the contrary, tetragonal (Ho, Lu, Y)PO_4 has no preferred growth direction in the crystalline phase based on their crystal structure [7]. When the concentration of citrate increasing from 0.5 to 5.0 mmoL, the hexagonal phase $YPO_4 \cdot 0.8H_2O$ obtained (see Fig. 6).

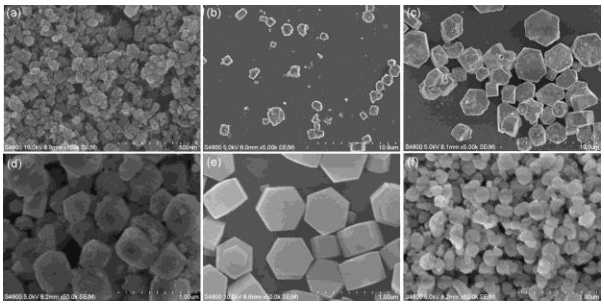

Fig. 5. FE-SEM images of YPO_4:Eu^{3+} products prepared with different concentration of Cit^{3-}: (a) 0.0 (b) 0.5 mmol (c) 1.0 mmol, (d) 2.0 mmol, (e) 2.2 mmol, (f) 5.0 mmol

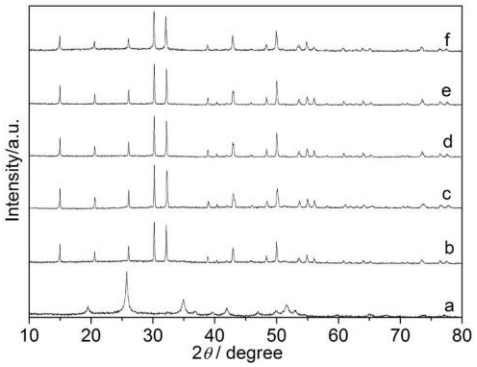

Fig. 6. XRD patterns of YPO_4:Eu^{3+} products prepared with different concentration of Cit^{3-}: (a) 0.0, (b) 0.5 mmol, (c) 1.0 mmol, (d) 2.0 mmol, (e) 2.2 mmol, (f) 5.0 mmol

3.4. Mechanism for the formation of the phase transformation

The above experiment results showed that the hexagonal phase YPO_4:Eu crystals obtained at a different amount of citrate and oxalate as organic additive. When no citrate/oxalate ions was added in the solution, the synthesized products can be indexed to the tetragonal structure YPO_4:Eu. It has been also reported that the synthesis of YPO_4 in aqueous media and organic solvent usually yields the tetragonal phase [30,31], whereas in our system the formation of the hexagonal phase is favoured by organic additives citrate/oxalate-introced.

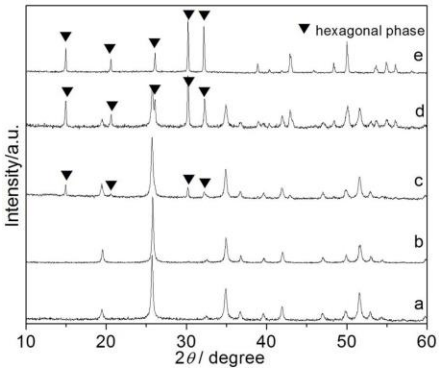

Fig. 7. XRD patterns of YPO_4:Eu^{3+} prepared with different concentration of ammonium benzoate: (a) 0.5 mmol, (b) 1.0 mmol, (c) 1.2 mmol, (d) 1.6 mmol, (e) 2.0 mmol

To understand the influencing of the capability of organic additives in the hexagonal structure, the products YPO_4:Eu subjected to ammonium benzoate as organic additive was studied by XRD patterns. Fig. 7a,b showed the XRD patterns of the products prepared with the concentration of benzoate were from 0.5 to 1.0 mmol. The tetragonal phase YPO_4 was obtained, without hexagonal phase was found. When the concentration of benzoate was 1.2 to 1.6 mmol, the mixed tetragonal and hexagonal phase appeared (Fig. 7c,d). While the concentration of benzoate reaching to 2.0 mmol, all reflection peaks in Fig. 7e could be indexed to hexagonal phase $YPO_4 \cdot 0.8H_2O$, no tetragonal phase could be observed. Table 1 shows that the structure of hexagonal YPO_4:Eu intensively depends on organic additives. Apparently, the charge and the concentration of organic additives will be influencing the phase transformation of YPO_4:Eu.

Table 1. The phase of the products prepared with different organic additives

Organic additives	The concentration of organic additives (mmol)	Valence state	Samples structrure
citrate	0.0		tetragonal phase
	0.2	-3	the mixed tetragonal and hexagonal phase
	0.5-5.0		hexagonal phase
oxalate	0.2		tetragonal phase
	0.5	-2	the mixed tetragonal and hexagonal phase
	0.7(12h)		the yttrium oxalate hydrate and hexagonal phase
	0.7(24h)		hexagonal phase
benzoate	0.5-1.0		tetragonal phase
	1.0-1.6	-1	the mixed tetragonal and hexagonal phase
	2.0		hexagonal phase

In a our earlier work [23], it is has been shown that the phase transformation of $CePO_4$ from hydrated hexagonal to dehydrated monoclic structure take place in through an oxalate-induced hydrothermal route. Multiple roles can be attributed to oxalate during the entire course of the synthesis: (i) $C_2O_4^{2-}$ served as ligand and chelating agent of the Ce^{3+} ions. It permits achieving control over the nuclear growth rate and obtaining samples of 1D growth, (ii) $C_2O_4^{2-}$ were absorbed on the surface of the initially formed hexagonal $CePO_4$ nanorods, which might result in the growth of initial monoclinic $CePO_4$ particles. Apparently, the capability of coordination of organic additives will be influencing the phase transformation of YPO_4 (Fig. 1).

For the same reason, the citrate/oxalate/benzoate ions possesse carboxylic functional groups, providing chelating ability. During the reaction, the citrate/oxalate/benzoate ions are used to chelate Y^{3+} through the carboxyl group, and then phosphate reacts with Y^{3+} to form YPO_4 (nucleation), which would slow-released the yttrium source. Then, the substituted citrate/oxalate/benzoate ions will be adsorbed to the surface of the initial formation of yttrium phosphates. It is quite possible that Cit^{3-} and $C_2O_4^{2-}$ are absorbed on the surface of the initially formed YPO_4:Eu particles around Y^{3+} cations, which might result in the growth of initial hexagonal $YPO_4 \cdot 0.8H_2O$ particles.

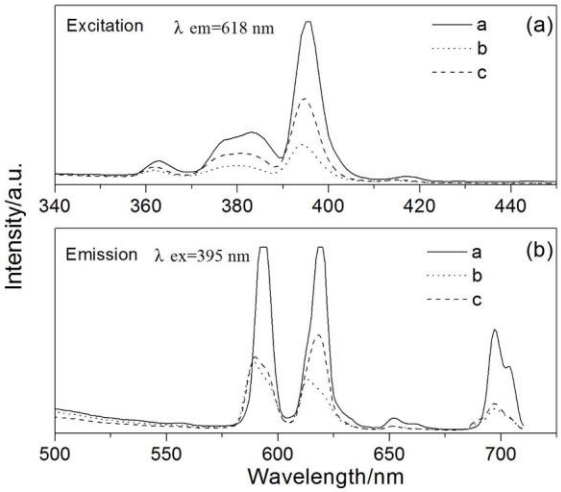

Fig. 8. The excitation (a) and emission spectra (b) of obtained YPO_4:Eu phosphors (full line: tetragonal phase, dashed line: hexagonal phase prepared with oxalate - induced, dotted line: hexagonal phase prepared with citrate-induced)

3.5. Luminescence study

The excitation and emission spectra are shown in Fig. 8a,b. When these species were excited at 395 nm, the emission spectrum (Fig. 8b) consist of sharp peaks at about 592, 617, 650, 696 nm, which are assigned to the transitions of $^5D_0 \rightarrow {}^7F_1$, $^5D_0 \rightarrow {}^7F_2$, $^5D_0 \rightarrow {}^7F_3$, $^5D_0 \rightarrow {}^7F_4$, respectively [32,33]. The highest integrated emission intensity is noted at the tetragonal phase YPO_4:Eu. The hexagonal phase YPO_4:Eu lead to weak to Luminescence, which might result from the hydroxyl quenching at the surfaces [34]. The emission line at 592 nm corresponding to the magnetic dipole transition $^5D_0 \rightarrow {}^7F_1$ of Eu^{3+} in the hexagonal phase prepared with citrate-induced, is much stronger than emission line at 614 nm assigned to the forced electronic dipole transition $^5D_0 \rightarrow {}^7F_2$ of Eu^{3+} from which we can conclude that Eu^{3+} occupied the lattice sites with symmetry. Additionally, it is observed that the ratio of relative intensity of the electronic dipole transition $^5D_0 \rightarrow {}^7F_2$ to the magnetic dipole transition $^5D_0$-$^7F_1$ in the samples of oxalate-introduced synthesis is larger than else samples, which reveal a lower symmetry of Eu^{3+} in a given host [35,36]. The difference in luminescence properties is possibly ascribed to the absorption of the residual $Y_2(C_2O_4)_3$ on the surface of the YPO_4:Eu, which might be to show a lower symmetry. To further confirm the residual $Y_2(C_2O_4)_3$ effects of the products, the IR spectra of analysis was performed (Fig. 3). And the luminescence properties are largely impacted by factors such as the different morphology, size and crystal structure [7,12].

4. Conclusion

In summary, the hexagonal phase YPO_4:Eu with nano/microsizes could be controlled by varying the concentration of the organic additives ions. The concentration of the citrate/oxalate/benzoate ions is found to play important roles in determining the morphologies and structures of YPO_4:Eu crystals. The citrate/oxalate/benzoate ions served as ligand and chelating agent of the Y^{3+} ions, which would slow-released the yttrium source. These substituted ions were absorbed on the surface of the initially formed tetragonal YPO_4 particles, resulting in the growth of hexagonal phase YPO_4. The $Y_{0.95}PO_4$:$Eu_{0.05}$ exhibit strong red photoluminescence.

Acknowledgment

This work was supported by the National Natural Science Foundation of China (No. 21266015); the National Natural Science Foundation of Inner Mongolia Autonomous Region (No. 2015MS0502 and 2015ZD01); and Research Program of science and technology at Universities of Inner Mongolia Autonomous Region (No. NJZY14008).

References

[1] G. Y. Adachi, N. Imanaka, Chem. Rev. **98**(4), 1479 (1998).
[2] S. P. Fricker, Chem. Soc. Rev. **35**(6), 524 (2006).
[3] S. L. Gai, C. X. Li, P. P. Yang, J. Lin, Chem. Rev. **114**(4), 2343 (2014).
[4] H. Mass, A. Currao, G. Calzaferri, Angew, Chem. Int. Ed. **41**, 2495 (2002).
[5] J. A. Dorman, J. H. Choi, G. Kuzmanich, J. P. Chang, J. Phys. Chem. C **116**(23), 12854 (2012).
[6] A. I. Becerro, S. Rodríguez-Liviano, A. J. Fernández-Carrión, M. Ocaña, Cryst. Growth Des. **13**(2), 526 (2013).
[7] Y. P. Fang, A. W. Xu, R. Q. Song, H. X. Zhang, L. P. You, J. C. Yu, H. Q. Liu, J. Am. Chem. Soc. **125**(51), 16025 (2003).
[8] Y. Ni, J. M. Highes, A. N. Mariano, Am. Mineral. **80**(1-2), 21 (1995).
[9] A. Hezel, S. D. Ross, J. Inorg. Nucl. Chem. **29**(8), 2085 (1967).
[10] P. Ghosh, A. Kar, A. Patra. J. Appl. Phys. **108**(11), 113506 (2010).
[11] Y. J. Zhang, H. M. Guan, J. Cryst. Growth **256**(1-2), 156 (2003).
[12] R. X. Yan, X. M. Sun, X. Wang, Q. Peng, Y. D. Li, Chem. Eur. J. **11**(7), 2183 (2005).
[13] S. Rodriguez-Liviano, F. J. Aparicio, C. R. Teresa, A. B. Hungría, L. Chinchilla, M. Ocaña, Cryst. Growth Des. **12**(2), 635 (2012).
[14] J. C. Chen, Q. G. Meng, S. P. May, T. Berry Mary, C. K. Lin, J. Phys. Chem. C **117**(11), 5953 (2013).
[15] Y. W. Zhang, Z. G. Yan, L. P. You, R. Si, C. H. Yan, Eur. J. Inorg. Chem. **2003**(22), 4099 (2003).
[16] A. Lecointre, A. Bessiere, A. J. J. Bos, P. Dorenbos, B. Viana, S. J. Jacquart, J. Phys. Chem. C **115**(10), 4217 (2011).
[17] M. N. Luwang, R. S. Ningthoujam, S. Jagannath, S. K. Srivastava, R. K. Vatsa, J. Am. Chem. Soc. **132**(8), 2759 (2010).
[18] M. N. Luwang, R. S. Ningthoujam, S. K. Srivastava, R. K. Vatsa, J. Am. Chem. Soc. **133**(9), 2998 (2011).
[19] H. X. Mai, Y. W. Zhang, L. D. Sun, C. H. Yan, Chem. Mater. **19**(18), 4514 (2007).
[20] M. F. Zhang, H. Fan, B. J. Xi, X. Y. Wang, C. Dong, Y. T. Qian, J. Phys. Chem. C **111**(18), 6652 (2007).
[21] Nuria O. Nuñz, Sonia R. Liviano, Manuel Ocaña, J. Colloid Interface Sci. **349**(2), 484 (2010).
[22] W. Di, J. Li, N. Shirahata, Y. Sakka, M. G. Willinger, N. Pinna, Nanoscale **3**, 1263 (2011).
[23] J. R. Bao, R. B. Yu, J. Y. Zhang, D. Wang, J. X. Deng, J. Chen, X. R. Xing, Scripta Mater. **62**(3), 133 (2010).
[24] J. R. Bao, R. B. Yu, J. Y. Zhang, X. D. Yang, D. Wang, J. X. Deng, J. Chen, X. R. Xing, Cryst. Eng. Comm. **11**(8), 1630 (2009).
[25] L. Bo, S. Liya, L. Xiaozhen, Z. Shuiche, Z. Yumeri, W. Tianmain, Y. Sasaki, K. Ishii, Y. Kashiwaya, H. Takahashi, T. Shibayama, J. Mater. Sci. Lett. **20**(11), 1071 (2001).
[26] G M. Begun, G W. Beall, L. A. Boatner, W. J. Gregor, J. Raman Spectrosc. **11**(4), 273 (1981).
[27] K. Rajesh, P. Shajesh, O. Seidel, P. Mukundan, K. G. K. Warrier, Adv. Funct. Mater. **17**(10), 1682 (2007).
[28] S. Lucas, E. Champion, D. Bernache-Assollant, G Leroy. Solid. State. Chem. **177**(4-5), 1312 (2004).
[29] N. K. Sahu, R. S. Ningthoujam, D. Bahadu, J. Appl. Phys. **112**(1), 014306 (2012).
[30] L. H. Zhang, G. Jia, H. P. You, K. Liu, M. Yang, Y. H. Song, Y. H. Zheng, Y. J. Huang, N. Guo, H. J. Zhang, Inorg. Chem. **49**(7), 3305 (2010).
[31] J. M. Nedelec, D. Avignant, R. Mahiou, Chem. Mater. **14**(2), 651 (2002).
[32] D. W. Wen, J. X. Shi, M. M. Wu, Q. Su, ACS Appl. Mater. Interfaces. **6**, 10792 (2014).
[33] M. Niraj Luwang, R. S. Ningthoujam, Jagannath, S. K. Srivastava, R. K. Vatsa, J. Am. Chem. Soc. **132**(8), 2759 (2010).
[34] W. H. Di, X. J. Wang, B. J. Chen, S. Z. Lu, X. X. Zhao, J. Phys. Chem. B **109**(27), 13154 (2005).
[35] P. Page, R. Ghildiyal, K. V. R. Murthy, Mater. Res. Bull. **41**(10), 1854 (2006).
[36] M. Kang X. M. Liao, Y. Q. Kang, J. Liu, R. Sun, G. F. Yin, Z. B. Huang, Y. D. Yao, J. Mater. Sci. **44**(9), 2388 (2009).

*Corresponding author: jinrongbao@imu.edu.cn, ranboyu@ustb.edu.cn